Developmental Cell
Article

External Mechanical Cues Trigger the Establishment of the Anterior-Posterior Axis in Early Mouse Embryos

Ryuji Hiramatsu,[1,2] Toshiki Matsuoka,[3] Chiharu Kimura-Yoshida,[1] Sung-Woong Han,[4] Kyoko Mochida,[1] Taiji Adachi,[4] Shuichi Takayama,[3] and Isao Matsuo[1,5,*]
[1]Department of Molecular Embryology, Osaka Medical Center and Research Institute for Maternal and Child Health, Osaka Prefectural Hospital Organization, 840 Murodo-cho, Izumi, Osaka 594-1101, Japan
[2]Department of Safety Research on Blood and Biological Products, National Institute of Infectious Diseases, 4-7-1 Gakuen, Musashi-Murayama, Tokyo 208-0011, Japan
[3]Department of Biomedical Engineering, University of Michigan, Ann Arbor, MI 48109, USA
[4]Department of Biomechanics, Institute for Frontier Medical Sciences, Kyoto University, 53 Kawaharacho, Shogoin, Sakyo, Kyoto 606-8507, Japan
[5]Department of Pediatric and Neonatal-Perinatal Research, Graduate School of Medicine, Osaka University, Suita, Osaka 565-0871, Japan
*Correspondence: imatsuo@mch.pref.osaka.jp
http://dx.doi.org/10.1016/j.devcel.2013.09.026

SUMMARY

Mouse anterior-posterior axis polarization is preceded by formation of the distal visceral endoderm (DVE) by unknown mechanisms. Here, we show by in vitro culturing of embryos immediately after implantation in microfabricated cavities that the external mechanical cues exerted on the embryo are crucial for DVE formation, as well as the elongated egg cylinder shape, without affecting embryo-intrinsic transcriptional programs except those involving DVE-specific genes. This implies that these developmental events immediately after implantation are not simply embryo-autonomous processes but require extrinsic factors from maternal tissues. Moreover, the mechanical forces induce a breach of the basement membrane barrier at the distal portion locally, and thereby the transmigrated epiblast cells emerge as the DVE cells. Thus, we propose that external mechanical forces exerted by the interaction between embryo and maternal uterine tissues directly control the location of DVE formation at the distal tip and consequently establish the mammalian primary body axis.

INTRODUCTION

Establishment of the three body axes, the anterior-posterior (A-P) axis, dorsal-ventral axis, and left-right (L-R) axis, is an essential event for proper mammalian embryogenesis. The mouse A-P axis is initially generated in a proximal-distal (P-D) direction at around 5.5 days postcoitum (dpc) prior to gastrulation. Notably, a distinct population of visceral endoderm (VE) cells marked by *Hex*, *Cer1*, and *Lefty1* expressions emerges at the distal tip of the egg cylinder in this process (Thomas et al., 1998; Shawlot et al., 2000; Torres-Padilla et al., 2007; Yamamoto et al., 2004; Takaoka et al., 2006). At this stage, the embryonic region of the mouse conceptus (Co) consists of only two tissue layers, the embryonic ectoderm (epiblast) and VE, and morphologically, the implanted blastocyst elongates along the P-D direction and transforms into an egg cylinder shape (Smith, 1985). Thereafter, this P-D axis is converted to the A-P direction (Beddington and Robertson, 1999); these unique cells known as the distal VE (DVE) migrate proximally to the prospective anterior side of the embryo and consequently form the anterior VE (AVE) at 6.5 dpc (Thomas and Beddington, 1996; Thomas et al., 1998; Srinivas et al., 2004). These unique AVE populations are understood to specify the anterior character by preventing the posteriorizing signals, such as *Wnt* and *Nodal*, and to indirectly facilitate forebrain development (Thomas and Beddington, 1996; Kimura et al., 2000; Perea-Gomez et al., 2002).

Several specific signaling pathways have been shown to be crucial players for the A-P axis polarization in mouse development. For example, Nodal/Activin signaling and Wnt signaling are required for correct DVE formation (Brennan et al., 2001; Chazaud and Rossant, 2006; Mesnard et al., 2006; Yamamoto et al., 2009), as well as AVE formation (Yamamoto et al., 2004; Kimura-Yoshida et al., 2005; Stuckey et al., 2011). Such molecular evidence is the result of powerful genetic studies and has contributed to our current understanding of the mechanism of A-P axis polarization (reviewed in Arnold and Robertson, 2009; Rossant and Tam, 2009). However, the mechanism of emergence of DVE cells, i.e., when and how these small numbers of cells express DVE markers in the distal tip, is still not well understood. In addition, the uterine environment, such as the spatial restriction at the implantation site and mechanical interaction between the embryo and the surrounding uterine tissue, should be considered. Although the relationship between the orientation of implantation and the future definitive axes of the embryos has been studied (Smith, 1985; Rossant and Tam, 2004; Mesnard et al., 2004), there is still little knowledge about how the uterine environment is involved in the establishment of body axes.

Recently, mechanical cues have been shown to contribute to several crucial biological events. A number of phenomena, such as cell shape- or substrate stiffness-mediated modulation of

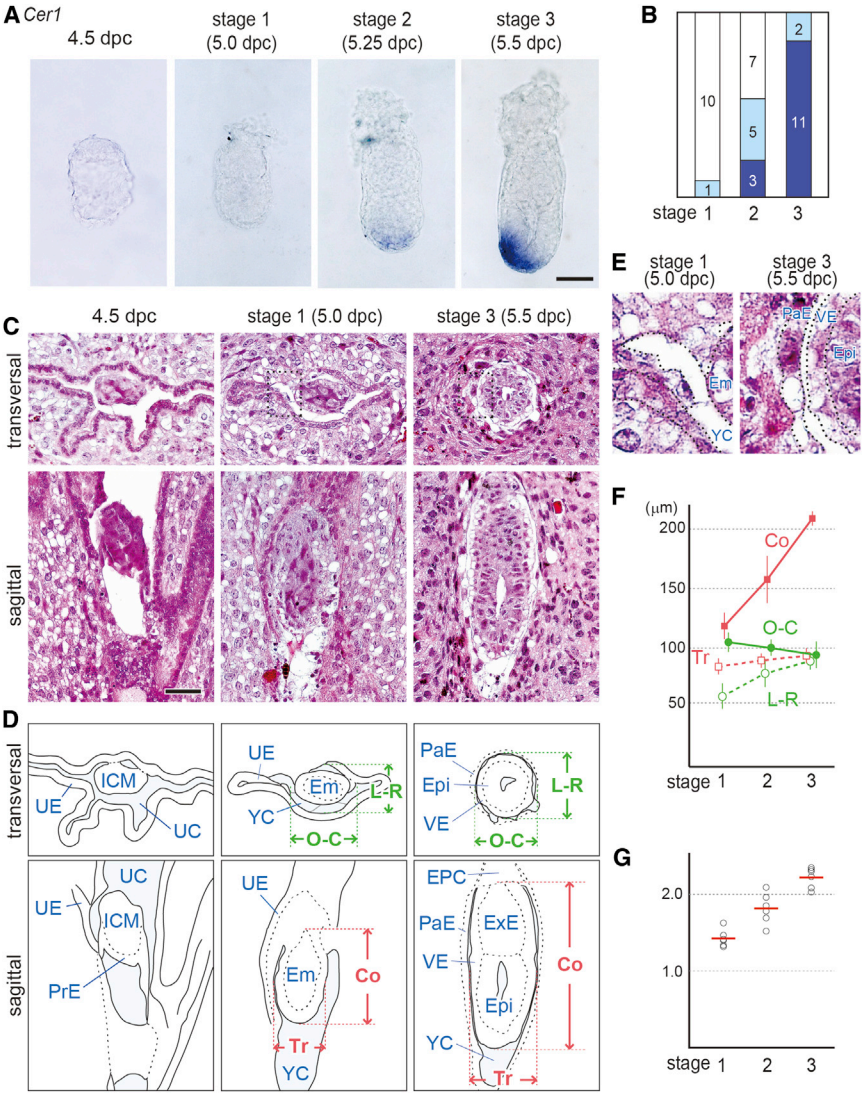

Figure 1. Morphological Profiles of Mouse Embryos during DVE Formation

(A and B) Whole-mount in situ hybridization of *Cer1* mRNA during 4.5–5.5 dpc. Distribution of the number of embryos showing three types of *Cer1* mRNA expression: not detected (white), detected slightly (light blue), and detected strongly (dark blue).

(C) Histological features of the embryos at 4.5 dpc, stage 1 (5.0 dpc), and 3 (5.5 dpc). Upper panels show the Tr sections, and lower panels show the sagittal sections of the embryos. Cells with vacuoles were abundantly found in the surrounding maternal tissues at 5.0 dpc; in contrast, the number of cells with vacuoles was decreased, and the squamous cells were prominently increased at 5.5 dpc.

(D) Schematic drawings of the histological views in (C). Co, the Co length between the boundary of the ectoplacental cone and the ExE and apex of the embryo; Tr, the Tr length at the level of the boundary between the epiblast and ExE; O-C, the length along the O-C axis of the yolk sac cavity; L-R, the length along the L-R axis of the yolk sac cavity; UE, uterine epithelium; UC, uterine cavity; YC, yolk sac cavity; ICM, inner cell mass; PrE, primitive endoderm; Em, embryonic region; Epi, epiblast; PaE, parietal endoderm; EPC, ectoplacental cone.

(E) Magnified views of the dashed rectangles in (C).

(F) Graph plotting the measurements of the lengths of the embryo proper and yolk sac cavity at stages 1, 2, and 3. Red lines indicate the Co (solid) and the Tr (dot) lengths of embryos. Green lines indicate the lengths of O-C axis (solid) and L-R axis (dot) of yolk sac cavity. The values are the mean ± SD.

(G) The ratio of the Co versus Tr lengths at stages 1, 2, and 3. Red lines indicate the mean value of each ratio.

Scale bars, 50 μm. See also Figure S1.

differentiation, cannot be explained by molecular factors alone. Mechanical and biochemical cues together appear to coordinate many developmental processes. The elucidation of fundamental links between mechanical forces and molecular pathways has led to a considerable enhancement in our understanding of embryogenesis (Mammoto and Ingber, 2010; Janmey and Miller, 2011). However, we have very limited information regarding the ways in which mechanical cues directly regulate fundamental developmental processes.

Here, we develop an in vitro culture method of implanted mouse embryos prior to DVE formation in engineered microcavities. This series of culture experiments reveals that the external mechanical cues exerted on the embryo are crucial for DVE formation as well as elongation of the egg cylinder shape in the mouse embryo immediately after implantation. Strikingly, external forces induce a localized breach of the basement membrane (BM) and subsequent BM transmigration of the epiblast cells into the VE layer at the distal portion of the embryo, without affecting embryo-intrinsic transcripts except DVE-specific genes. Consequently, the migrated epiblast cells appeared to become DVE/AVE cells. Thus, we propose that external mechanical forces at the peri-implantation stage directly trigger the establishment of the A-P axis polarity, one of the fundamental processes of mammalian embryogenesis.

RESULTS

Morphological Profiles of the Mouse Concepti during DVE Formation

To accurately determine the morphological profiles of mouse concepti during DVE formation, we reexamined the temporal expression patterns of DVE markers (Figure 1A; see Figure S1C available online). We classified the embryos between 5.0 and 5.5 dpc into the following three stages morphologically under a dissecting microscope: stage 1, the proamniotic cavity is not observed clearly (5.0 dpc); stage 2, the proamniotic cavity is clearly visible, but the VE is not thickened at the distal tip (5.25 dpc); stage 3, both the proamniotic cavity and thickened DVE are evident (5.5 dpc; Figure S1A). *Cer1* mRNA expression was not observed in embryos at 4.5 dpc (Figure 1A) and in

most of the embryos at stage 1 (Figures 1A and 1B). *Cer1* expression began to be detectable in the distal tip of some embryos around stage 2 (Figures 1A and 1B). At stage 3, *Cer1* expression was detected strongly in the distal tips of most embryos (Figures 1A and 1B). *Hex* transcripts, the other marker of the DVE, also displayed similar temporal expression profiles at stages 1, 2, and 3 (Figures S1C and S1D), whereas they were detected throughout the primitive endoderm at 4.5 dpc, as shown previously (Figure S1C; Thomas et al., 1998). These findings coincide with the idea that DVE formation is established at around stage 3, at 5.5 dpc (Thomas et al., 1998; Kimura et al., 2000; Mesnard et al., 2006).

Next, we histologically examined the morphological characteristics of concepti, including the maternal tissues, at these stages (Figures 1C, 1D, and S1B). At 4.5 dpc, upon implantation, the embryo exhibited a blastocyst-like shape, and the mural trophoblast layer was attached to the uterine epithelium. The uterine epithelium layer was observed clearly, and the uterine cavity surrounded the embryo. The hinge regions of the uterine epithelium were not fused. At stage 1 (5.0 dpc), the embryo grew into an early egg cylinder-like shape (bowl-like shape), and the yolk sac cavity surrounded the embryo. The uterine epithelium layer was still partially detectable. The yolk sac cavity had a protruding portion on each side, and the hinge regions of the uterine epithelium were fused partially, but incompletely (Figure 1E). At stage 3 (5.5 dpc), the embryo proper, including the epithelial layer of the epiblast and the proamniotic cavity, was elongated along the P-D direction. The space of the yolk sac cavity was only observed at the distal side of the embryo. The uterine epithelium layer was not clearly observed, and the protruding part of the uterine cavity at each side of the embryo had disappeared, with the cavity surrounding the embryo forming a tubular shape (Figure 1E). These histological observations are largely compatible with those reported in the earlier literature (Potts 1968; Smith 1985).

To describe the egg cylinder shape more quantitatively, we measured the size of the embryo during these stages (Figure 1F). The mean values of the Co lengths, which were the distances between the distal end of the embryo and the border of the extraembryonic ectoderm (ExE) and ectoplacental cone, were 118.9 ± 11.2 μm at stage 1, 157.7 ± 19.9 μm at stage 2, and 209.4 ± 6.1 μm at stage 3 (Figures 1D and 1F, Co). In contrast, the mean values of transversal (Tr) lengths at the embryonic region were 84.3 ± 6.7 μm at stage 1, 89.5 ± 6.0 μm at stage 2, and 93.5 ± 6.3 μm at stage 3 (n = 6; Figures 1D and 1F, Tr). The average ratios of the Co length per Tr length were 1.40 at stage 1, 1.75 at stage 2, and 2.24 at stage 3 (Figure 1G). These results indicate that the Tr lengths increase slightly, whereas the Co length of the embryo becomes approximately 1.8 times longer during this period. Hence, the difference in the growth rates along the sagittal axis and Tr axis gives rise to the elongated shape of the egg cylinder at 5.5 dpc from the bowl-like shape at 5.0 dpc during DVE formation.

To address why the Tr length shows little increase, whereas the Co length shows substantial increase, we also measured the Tr length of the yolk sac cavity surrounding the embryo. The means of the lengths along the oviduct-cervix (O-C) axis of the yolk sac cavity were 105.0 ± 8.3 μm at stage 1, 100.3 ± 6.8 μm at stage 2, and 94.2 ± 11.2 μm at stage 3 (Figures 1D and 1F, O-C). In addition, the means of the lengths along the L-R axis of the yolk sac cavity were 59.2 ± 10.7 μm at stage 1, 78.7 ± 11.9 μm at stage 2, and 88.4 ± 7.2 μm at stage 3 (n = 7; Figures 1D and 1F, L-R). These results show that the length of the yolk sac cavity along the O-C axis is decreased, and the length along the L-R axis is increased, whereas the change of these lengths is not prominent, compared with the Co length of the embryo. Consequently, the lengths of the yolk sac cavity along the O-C and L-R axes and the Tr length of the embryo appear to converge at 90–100 μm. These histological observations suggested the possibility that the yolk sac cavity formed by the maternal tissues and parietal endoderm may restrict the growth of the embryo proper along the Tr axis to elongate the egg cylinder shape during DVE formation.

External Spatial Restriction of the Embryo Is Necessary for A-P Axis Formation In Vitro

To investigate whether confinement per se by the yolk sac cavity is important for elongation of the egg cylinder shape and DVE formation, we engineered an artificial yolk sac cavity device by creating a microcavity inside of an elastomer called PDMS (polydimethylsiloxane; Sylgard 184). Two microcavity designs with different diameters were constructed: a narrower cavity of 90 μm in diameter, which matches the length of the yolk sac cavity along the O-C and L-R axis at stage 3; and another wider cavity of 180 μm in diameter, which is twice the length. Then, stage 1 embryos were inserted into these two differently sized microcavities in the culture medium (Figures 2A and 2B).

First, to determine whether the cavity can realize the change from the bowl-like to elongated shape of the egg cylinder, we measured the Co and Tr lengths of the embryo cultured in the microcavities for 8 hr (Figure 2C). After the culture in the narrow cavity, the Co length became 192.8 ± 15.7 μm, and the Tr length became 89.6 ± 4.1 μm. In contrast, after the culture in the wide cavity, the Co length (138.1 ± 9.7 μm) was smaller, whereas the Tr length (102.9 ± 6.7 μm) was larger compared with those in the narrow cavity (n = 9; Figures 2D and 2E). The ratio of Co lengths versus Tr lengths for embryos cultured in the narrow cavity was 2.15, which is similar to that for the embryos at stage 3 in vivo and can be considered to constitute the elongated shape. Conversely, the ratio for embryos cultured in the wide cavity was only 1.34, which is comparable to that of embryos at stage 1 in vivo and can be considered to constitute the bowl-like shape (Figure 2F). In addition, the total cell numbers for the epiblast, VE, and ExE were not changed significantly between the embryos cultured in the narrow and wide cavities for 8 hr (313.25 ± 15.56 and 315.75 ± 14.48, respectively; n = 4; Figure S2A). Together, these results show that the microcavity can change the egg cylinder shape, but not the total cell number, and also suggest that without this external cue, the embryo cannot elongate the egg cylinder shape autonomously in vitro.

Considering that DVE formation is established at stage 3 and that DVE tends to be apparent only after the egg cylinder has reached a critical minimal size of 180 μm in the Co length of the embryo (Mesnard et al., 2006), we next explored whether the cavity can also affect DVE formation. *Cer1* mRNA expression was detected at the distal tips of most of the embryos cultured in the narrow cavity for 8 hr (Figures 2G and 2H). In contrast, *Cer1* expression was hardly detectable in embryos cultured in the

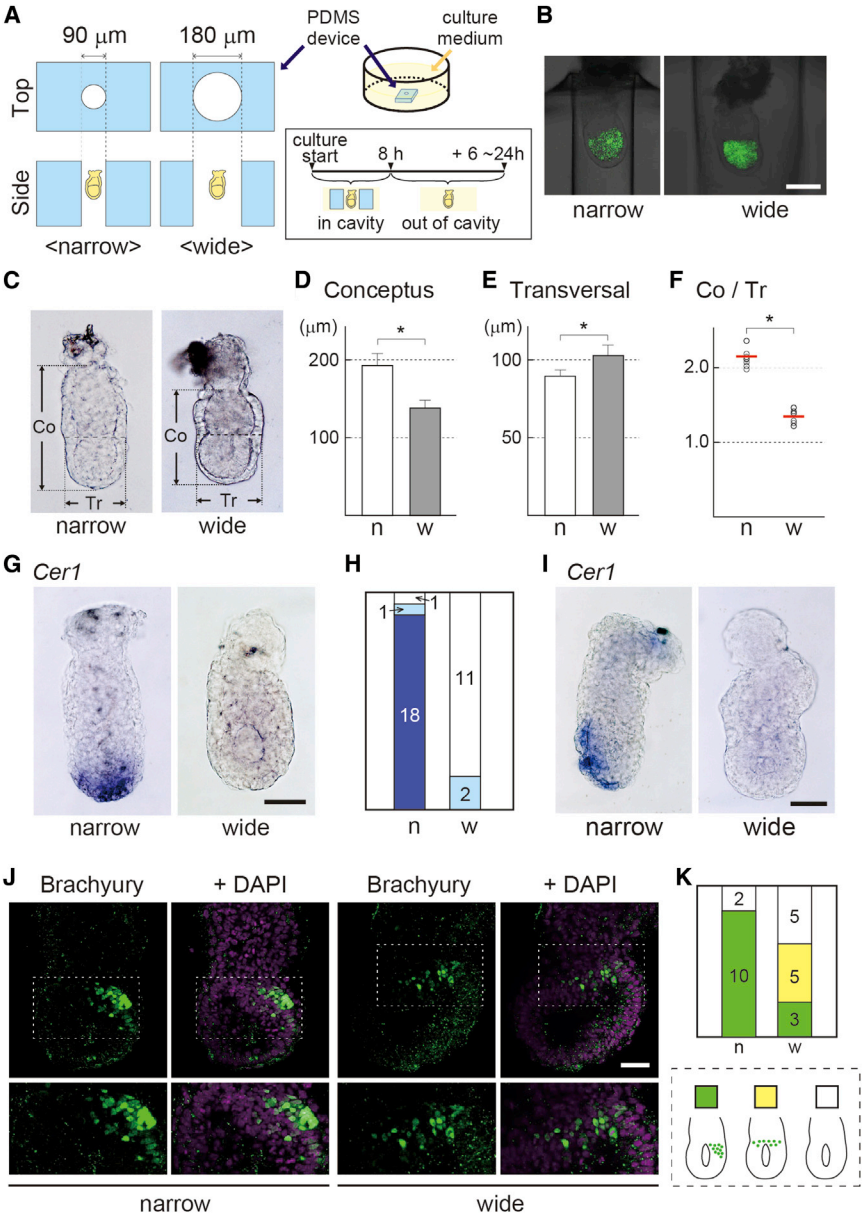

Figure 2. External Spatial Restriction Is Required for Proper Formation of the A-P Axis In Vitro

(A) A schematic representation showing the embryo culture in the microcavity with the PDMS device.

(B) Confocal images showing *Sox2-Venus* transgenic embryos (epiblast in green) at 5.0 dpc in the "narrow" and "wide" microcavity devices.

(C) Eight-hour-cultured embryos in the narrow cavity (left) and in the wide cavity (right).

(D and E) The average of the Co (D) and Tr (E) lengths of the embryo from the narrow cavity (n) and the wide cavity (w). The values are the mean ± SD.

(F) The ratio of the Co versus the Tr lengths in the narrow cavity and the wide cavity. Red lines indicate the mean value of each ratio.

(G and H) Whole-mount in situ hybridization of *Cer1* mRNA in 8-hr-cultured embryos in the narrow cavity (left) and in the wide cavity (right). Distribution of the number of embryos from the narrow cavity and wide cavity shows three types of *Cer1* mRNA expression (H): not detected (white), detected slightly (light blue), and detected strongly (dark blue).

(I) Whole-mount in situ hybridization of *Cer1* mRNA of additional 6-hr-cultured embryos from the narrow cavity (left) and from the wide cavity (right).

(J and K) Immunohistochemical analysis of anti-Brachyury (green) merged with DAPI (nuclei, magenta) in the embryo from the narrow cavity (left) and from the wide cavity (right) cultured for 24 hr. The lower panels show higher magnifications of the areas in the upper panels (J). Distribution of the number of embryos from the narrow cavity and wide cavity shows three types of Brachyury localization: restricted to one side of the proximal region (green), observed broadly in the proximal region (yellow), and negative (white). In the lower dashed rectangle, schematic images of the three types are illustrated.

Scale bars, 50 μm. *p < 0.01. See also Figure S2.

wide cavity for 8 hr (Figures 2G and 2H). Additionally, the expressions of *Hex*, *Lefty1*, and *Foxa2*, the other DVE markers, were also detected at the distal tips of the embryos cultured in the narrow cavity, whereas they were not detected in those cultured in the wide cavity device (Figures S2B–S2D). These results indicate that external restriction of the Tr embryo expansion is necessary for DVE formation in vitro.

To further examine whether the subsequent axis rotation, i.e., the anterior migration of DVE cells and posterior shift of primitive streak markers, can take place in the cultured embryos, we analyzed *Cer1* expression in embryos that were subjected to 8 hr culture in the microcavity followed by an additional 6 hr of culture outside of the cavity (Figure 2A). In embryos from the narrow cavity, the *Cer1*-positive area was observed at one proximal side (Figure 2I). In contrast, *Cer1* expression was not observed in most of the embryos from the wide cavity, which was consistent with the above findings (Figures 2G–2I). Additionally, we assessed the Brachyury localization, a posterior marker, in embryos cultured for 8 hr in the microcavity device followed by an additional 24 hr outside of the cavity (Figure 2A). The Brachyury protein was restricted to one side of the proximal region at the embryonic/extraembryonic boundary in most of the embryos from the narrow cavity (Figures 2J and 2K). Conversely, the Brachyury expression was scattered or undetected in the majority of embryos from the wide cavity device (Figures 2J and 2K). These results indicate that the P-D axis can be converted to the future A-P axis in the embryos from the narrow cavity. Taken together with the aforementioned findings, these results indicate that external restriction of the embryo expansion is necessary for proper formation of the A-P axis polarity immediately after implantation in vitro.

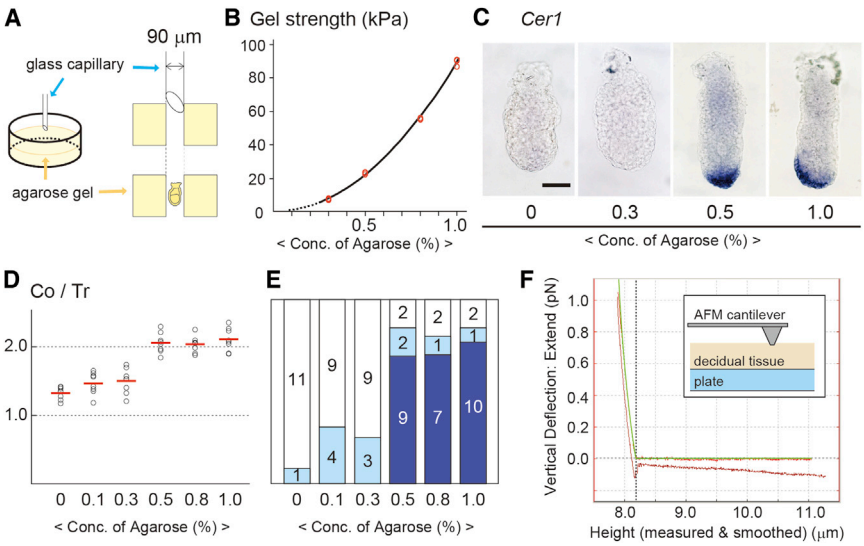

Figure 3. Sufficient External Force Is Required for Proper Formation of the A-P Axis In Vitro

(A) A schematic representation showing the embryo culture in the microcavity with the agarose gel.

(B) Graph plotting the gel strengths of each concentration (Conc.) of agarose gel (0.3%, 0.5%, 0.8%, and 1.0%). R-square of the trend line ($y = 88.7\ x^2$) is 0.998.

(C) Eight-hour-cultured embryos in 0%, 0.3%, 0.5%, and 1.0% agarose gel.

(D) The ratio of the Co versus the Tr lengths in 0%, 0.1%, 0.3%, 0.5%, 0.8%, and 1.0% gel. Red lines indicate the mean value.

(E) The number of embryos cultured in 0%, 0.1%, 0.3%, 0.5%, 0.8%, and 1.0% gel showing three types of *Cer1* mRNA expression: not detected (white), detected slightly (light blue), and detected strongly (dark blue).

(F) The force curve collected from a decidual tissue. The inset schematic representation shows the AFM probe indenting a decidual tissue on a plate. Scale bar, 50 μm. See also Table S1.

Sufficient External Strength Surrounding the Embryo Is Necessary for the DVE Formation

To further investigate the confinement as an external mechanical cue to promote the formation of the elongated egg-cylinder shape and the DVE, we prepared microcavities (90 μm in diameter) formed inside agarose gels of different stiffness prepared by varying the gel concentration (0%, 0.1%, 0.3%, 0.5%, 0.8%, and 1.0%) and then inserted stage 1 embryos into the cavities (Figure 3A). First, we measured the modulus of the different concentrations of agarose gels. The modulus was 7.29 ± 0.44 kPa for 0.3%, 22.94 ± 0.66 kPa for 0.5%, 55.49 ± 0.50 kPa for 0.8%, and 89.45 ± 2.17 kPa for 1.0% (the mean ± S.D.; 0.1%, not measurable; Figure 3B) agarose gel. These moduli increased with the square of the concentration of agarose gel.

To determine whether the external strength can affect the change from the bowl-like to elongated shape of the egg cylinder, we measured the Co and Tr lengths of embryos cultured in the microcavities formed inside varying concentrations of agarose (Figure 3C). After 8 hr of culture, the ratios of the Co lengths versus Tr lengths for embryos cultured in 0%, 0.1%, and 0.3% agarose gel were 1.32, 1.46, and 1.51, respectively (Figure 3D), which are comparable to that of embryos at stage 1 in vivo. Conversely, the ratios for embryos cultured in 0.5%, 0.8%, and 1.0% gel were 2.05, 2.02, and 2.10, respectively (Figure 3D), which are comparable to that of embryos at stage 3 in vivo and considered to represent the elongated shape. Then, we investigated whether the gel moduli can also induce DVE formation and found that *Cer1* expression was hardly detectable in embryos cultured in 0%, 0.1%, and 0.3% agarose gel for 8 hr (Figures 3C and 3E). Consistent with the critical concentration of agarose gel for the elongated shape, *Cer1* expression was detected at the distal tips of the embryos cultured in 0.5%, 0.8%, and 1.0% gels for 8 hr (Figures 3C and 3E). These results show that agarose gels prepared with concentrations above 0.5%, which correspond to over 22.94 kPa stiffness, can promote the elongated shape of the egg cylinder as well as DVE formation. In contrast, the gels prepared with concentrations of 0.3% and below, i.e., under 7.29 kPa stiffness, were not capable of inducing an elongated shape of the egg cylinder or DVE formation.

To investigate whether sufficient stiffness of agarose gels for DVE formation can recapitulate the stiffness of maternal tissues surrounding the embryo in vivo, we measured the mechanical rigidity of decidual tissue by a force probe using an atomic force microscope (AFM) cantilever (Figure 3F). Data were averaged over multiple locations within each decidual surface isolated at 5.5 dpc (n = 6; 15 locations per sample and 90 in total). The average module of the decidual surface was 23.26 ± 9.8 kPa (the mean ± SD). Considering that the stiffness of soft tissue such as muscles is 10–20 kPa (Engler et al., 2004), the decidua could be considered comparable to the soft tissues in stiffness. This result suggests that the stiffness of gels that is sufficient for DVE formation is equal to the stiffness of the maternal tissues surrounding the embryo in vivo. Taken together with the aforementioned findings, these results indicate that confinement by a sufficiently stiff external environment is required for proper formation of the elongated egg cylinder shape and DVE formation.

Next, we performed a microarray analysis to identify the differences between the embryos cultured in the narrow and wide cavities for 8 hr. Transcriptional profiles under each culture condition revealed that only eight genes showed significant increases in the embryos cultured in the narrow cavity ($p < 0.05$); the increase was between 1.2- and 1.3-fold for seven of these genes, and 1.62-fold for *Cer1* (Table S1; microarray data base GSE51198). Four of the genes, *Cer1*, *Lefty1*, *Fzd5*, and *Fzd8*, were expressed in the DVE at 5.5 dpc (Figure 1A; Yamamoto et al., 2004, Lu et al., 2004; Kemp et al., 2007). Additional whole-mount in situ hybridization studies confirmed that no distinct differences in the expression patterns of markers for the epiblast, ExE, or extraembryonic VE were detectable (Figures S2E–S2J). These gene expression analyses indicated that there is no significant difference between the embryos cultured in the narrow and wide cavity devices in terms of embryo-intrinsic gene transcription, with the exception of DVE markers.

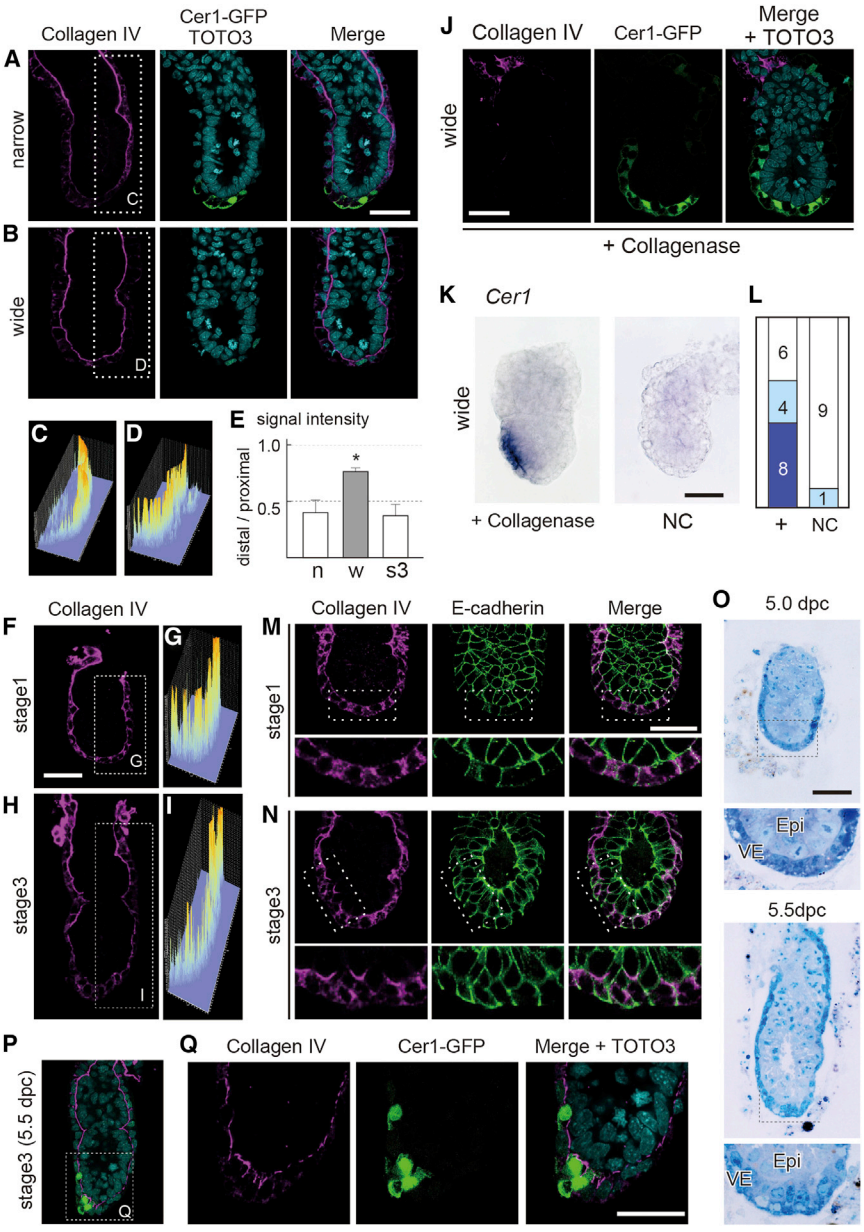

Figure 4. The BM Is Breached at the Distal Region during DVE Formation

(A and B) Immunohistochemical analysis of anti-collagen IV (magenta) merged with TOTO3 (nuclei, cyan) and Cer1-EGFP (DVE cells, green) in the embryo cultured in the narrow (A) and wide (B) cavity devices for 8 hr.

(C and D) The intensity of confocal images obtained by collagen IV immunohistochemical analysis in (A) and (B) is graphically depicted in three dimensions.

(E) The ratio of signal intensity of collagen IV at the distal region versus at the proximal region of the embryos cultured in narrow cavity (0.399 ± 0.111) and the wide cavity (0.762 ± 0.030) and isolated at stage 3 (5.5 dpc; s3; 0.372 ± 0.099). The values are the mean ± SD. *$p < 0.01$.

(F and H) Immunohistochemical analysis of anti-collagen IV (magenta) at 5.0 dpc (F) and 5.5 dpc (H).

(G and I) Intensity of confocal images obtained by collagen IV immunohistochemical analysis in (F) and (H) is graphically depicted in three dimensions.

(J) Immunohistochemical analysis of anti-collagen IV (magenta) merged with TOTO3 (nuclei, blue) and Cer1-EGFP (green) in the embryo cultured in the wide cavity with collagenase D for 8 hr.

(K) Whole-mount in situ hybridization of *Cer1* mRNA from the wide cavity with collagenase D.

(L) Distribution of the number of embryos showing *Cer1* expression with (left, +) or without (right, NC) collagenase D. The expression patterns of *Cer1* mRNA were classified into three types: not detected (white), detected slightly (light blue), and detected strongly (dark blue).

(M and N) Immunohistochemical analysis of anti-collagen IV (magenta) and anti-E-cadherin (green) at 5.0 dpc (M) and 5.5 dpc (N). The lower panels show higher magnifications of the areas in the upper panels.

(O) Histological analysis of semithin plastic sections stained with toluidine blue at 5.0 dpc (upper panels) and 5.5 (lower panels) dpc.

(P and Q) Immunohistochemical analysis of anti-collagen IV (magenta) merged with TOTO3 (nuclei, cyan) and Cer1-EGFP (DVE cells, green) at 5.5 dpc.

(Q) Higher magnifications of the areas in (P).

Scale bars, 50 μm. See also Figure S3.

The BM Is Breached in the Vicinity of Emerging DVE Cells

To explore differences between the embryos cultured in the narrow and wide cavities, we performed histological and molecular marker analyses and found that the deposition of the BM was altered between the two conditions. Histological observations revealed that boundaries of the epiblast and VE layers were obscure in the embryos cultured in the narrow cavity, whereas distinct boundaries were evident in the embryos cultured in the wide cavity (Figures 2C and S3A). To characterize the different features of the boundary more precisely, we evaluated how the BM is deposited between the two layers by immunohistochemistry of collagen IV, a major component of the BM (Figures 4A–4E). In embryos cultured in the narrow cavity, collagen IV was heavily deposited in the proximal BM but tended to be thinned in the distal BM (Figures 4A and 4C). Conversely, in the embryo cultured in the wide cavity, collagen IV appeared to be deposited heavily throughout the BM but not to be thinned even at the distal tip (Figures 4B and 4D). The ratio of the signal intensity of collagen IV in the distal BM to that in the proximal BM was significantly higher in the embryos cultured in the wide cavity than in those cultured in the narrow cavity (n = 4; Figure 4E). These results indicate that the narrow cavity device allows the embryo to thin out the BM deposition between the epiblast and VE in the distal region locally.

To assess whether this BM deposition is actually changed during normal DVE formation, we examined the spatiotemporal profiles of collagen IV protein during DVE formation in vivo. At 4.5 and 4.75 dpc, the time of implantation, collagen IV protein was strongly localized in all of the primitive endoderm cells but did

not display the BM-like deposition (Figure S3B). Subsequently, at stage 1, collagen IV protein appeared to be deposited in the BM between the epiblast/ExE and VE layers; moreover, it was heavily deposited in the distal portion of the BM (Figures 4F and 4G). At stage 3, in contrast, the collagen IV deposition was thinned at the distal tip locally, which closely resembles the collagen IV pattern of cultured embryos in the narrow cavity (Figures 4E, 4H, and 4I). These spatiotemporal patterns of BM deposition were consistently found with the antibodies for other extracellular matrix molecules, including heparin sulfate and nidogen (Shimokawa et al., 2011; R.H. and I.M., unpublished data).

To test whether the BM deposition is involved in localized DVE formation in vitro, we utilized collagenase D, which disassembles collagen IV protein (Figure 4J). Indeed, collagen IV and other BM proteins such as heparan sulfate were dramatically decreased by the collagenase treatment in embryos cultured in the wide cavity for 8 hr (Figure 4J; R.H. and I.M., unpublished data). Then, we assessed whether disassembly of the BM can induce DVE formation ectopically and found that *Cer1* expression was observed in the majority of collagenase-treated embryos even in the wide cavity (Figures 4J–4L); moreover, the *Cer1*-positive region was not restricted to the distal portion of the embryos but rather was broadly expanded in the VE layer (Figures 4J and 4K). On the other hand, *Cer1* expression was not evident in the cultured embryos without collagenase D (Figure 4L). These results suggest that the local thinning of the BM deposition may be correlated with the emergence of *Cer1*-positive cells in vitro.

We next examined the cellular morphology, including the cell shape, at the distal tip of the embryo more precisely using E-cadherin and collagen IV. At stage 1, the BM at the distal tip was deposited continuously, and the VE cells in the vicinity of this region were squamous or cuboidal, aligned in order, and formed a single layer (Figure 4M). At stage 3, in contrast, the BM was breached in the distal portion locally, and the surrounding VE cells displayed various shapes, not only squamous or cuboidal. Accordingly, these cells appeared to form not a simple epithelial layer but a layer of VE cells nested with epiblast cells in the vicinity of BM breaches (Figure 4N). A similar tendency toward morphological nesting was evident by fine structural analysis with toluidine blue-stained semithin sections (Figure 4O). These morphological studies revealed that the BM is breached at the distal region of the embryo locally when DVE is formed.

To further evaluate whether DVE formation is closely associated with the BM breaches, we examined the BM in the embryos of *Cer1-EGFP* transgenic mice (Mesnard et al., 2004; Kimura-Yoshida et al., 2005). At stage 3, when a couple of Cer1-EGFP-positive cells emerged at the distal tip, most of the Cer1-EGFP-positive cells (or the Cer1-EGFP-positive portion) appeared to be coherent with the BM breaches (n = 5; Figures 4P and 4Q). Taken together with the aforementioned findings, these results suggest that the BM breaches are intimately linked to the emergence of Cer1-positive DVE cells.

Epiblast Cells Transmigrate into the VE Layer and Contribute to the *Cer1*-Positive DVE

Because the distally localized BM breaches suggest that interactions between the epiblast and VE cells are crucial for DVE formation, we traced the fate of the epiblast-derived cells with *Sox2-cre* transgenic mice crossed to the *Rosa26R*$^{lacZ/+}$ reporter strain (Hayashi et al., 2002; Soriano 1999). At stage 1 (5.0 dpc), the epiblast lineages marked by β-galactosidase (β-gal) were exclusively observed in the epiblast layer, but not in the VE layer (Figures 5A and 5A′). However, at stage 3 (5.5 dpc), the β-gal-positive cells were observed in the VE layer at the distal portion in addition to the epiblast layer (Figures 5B and 5B′). The number of β-gal-positive cells in the VE layer was one to four at stage 3 (3.2 ± 0.84 cells, n = 5). At 6.0 dpc, the β-gal-positive cells were consistently observed in the proximal region and morphologically presumed to form the anterior side of the VE layer in the vicinity of the boundary between the epiblast and ExE (Figures 5C and 5C′). In some embryos, the β-gal-positive cells were observed on the extraembryonic VE portion beyond the boundary between the epiblast and ExE. At 6.5 dpc, in addition to the anterior side, the β-gal-positive cells had emerged into the opposite, posterior side, i.e., the primitive streak-derived mesendoderm (Figures 5D and 5D′). The number of β-gal-positive cells on the anterior side of the VE was approximately four at 6.5 dpc (4.2 ± 1.48 cells, n = 5). Moreover, double staining with Cer1 products and β-gal revealed that some of the β-gal-positive cells within the anterior side also expressed Cer1 (Figure 5E, arrows). However, β-gal-negative and Cer1-positive cells were also consistently observed (Figure 5E, arrowheads). Taken together, these results demonstrated that the transmigrated epiblast cells contributed to the DVE and subsequently the AVE.

To further investigate the behaviors of the epiblast cells, we generated *Sox2-Venus* transgenic mice, which allowed us to label the epiblast cells in living embryos (Figure 5F). We then observed the movement of Venus-positive cells of the living embryos dissected at stage 1 and cultured for 5–7 hr in the narrow or wide cavity devices. At the beginning of the culture (0 hr), Sox2-Venus expression was not detected in the VE layer, which showed positive for wheat germ agglutinin (WGA), of the embryo cultured in either the narrow or wide cavity devices. In the embryo cultured in the narrow cavity, the Sox2-Venus signal protruded from the epiblast into the WGA-positive VE layer at approximately 1 hr after the Tr length of the embryo reached the diameter of the cavity. Subsequently, the Sox2-Venus signal moved to the more apical side of the VE layer (Figure 5G). Coincidentally, the examination with in situ hybridization for this identical embryo revealed that the DVE region in the vicinity of the protruded Venus signal expressed *Cer1* transcripts (Figure 5H). However, in the embryo cultured in the wide cavity, no Sox2-Venus signal invaded into the VE layer throughout the 7 hr culture, and *Cer1* mRNA was also not expressed during this period (Figures 5I and 5J).

To investigate whether this cell movement takes place in vivo and is linked to breaches of BM, we examined the behaviors of the Sox2-Venus signal in the transgenic embryo during normal DVE formation (Figure 6A). Initially, at stage 1 (5.0 dpc), the Venus signal was restricted within the epiblast layer. Later, at stage 3 (5.5 dpc), the Sox2-Venus signal was also detected in the VE layer in the distal region beyond the BM (Figure 6A). Moreover, the Venus signals protruding into the VE layer were consistently found in the vicinity of the BM breaches (n = 8; Figures 6A and 6B). These observations are clearly supportive of behaviors of epiblast-derived cells in the embryos cultured in the narrow cavity device. Taken together with the aforementioned findings, these results show that external mechanical

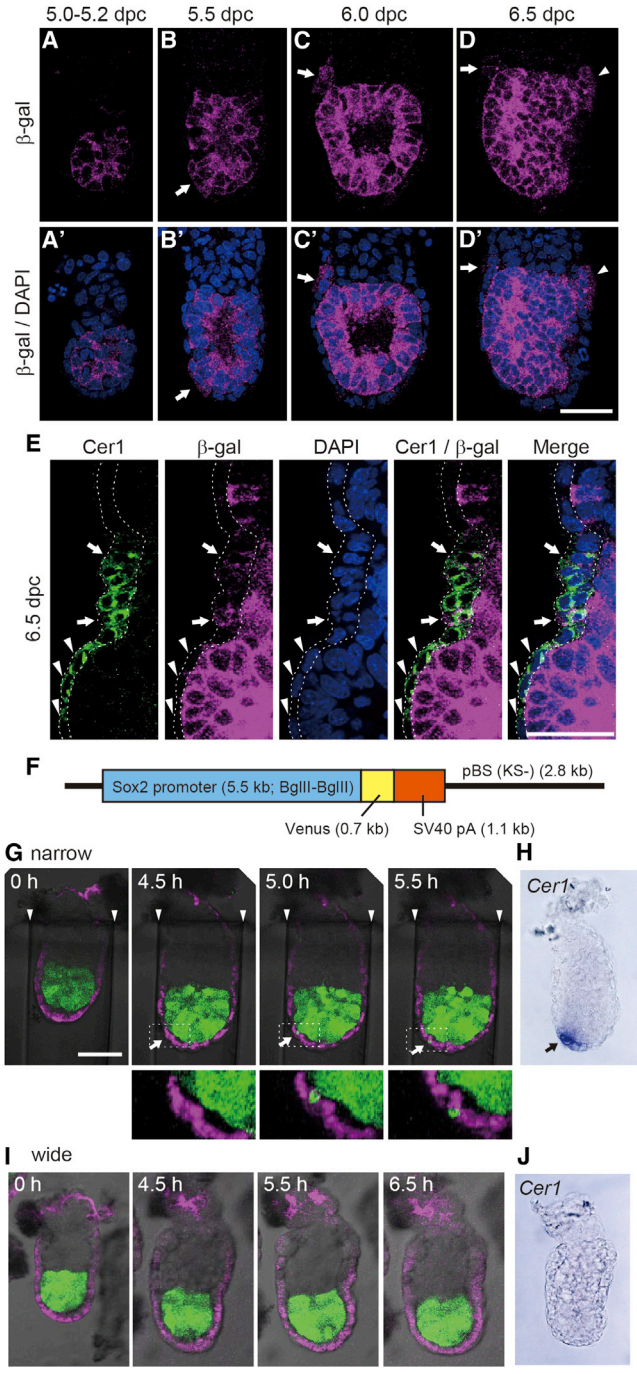

Figure 5. Behaviors of Cells Emigrated from the Epiblast into the VE Layer during DVE Formation

(A–D′) Immunohistochemical analysis of anti-β-gal (magenta) in *Sox2-cre*; *Rosa26R*$^{lacZ/+}$ embryos at 5.0–5.2 dpc (A and A′), 5.5 dpc (B and B′), 6.0 dpc (C and C′), and 6.5 dpc (D and D′). Merged images of β-gal antibody (magenta) with DAPI (nuclei, blue). Arrows indicate β-gal-positive VE cells, and arrowheads indicate primitive streaks.

(E) Immunohistochemical analysis of anti-Cer1 (green) and anti-β-gal (magenta) merged with DAPI (nuclei, dark blue) in *Sox2-cre*;*Rosa26R*$^{lacZ/+}$ embryos at 6.5 dpc. Arrows indicate Cer1-positive and β-gal-positive cells. Arrowheads indicate Cer1-positive and β-gal-negative cells.

(F) Schematic representation of the *Sox2-Venus* transgene construct.

(G and I) Time-lapse observation of *Sox2-Venus* transgenic embryos cultured in the narrow (G) and wide (I) cavity devices for 5.5–6.5 hr. Sox2-Venus (epiblast, green) and WGA (VE layer, magenta). Arrows indicate the protrusion of the Sox2-Venus signal. The lower panels show higher magnifications of the areas in the upper panels in (G).

(H and J) Whole-mount in situ hybridization of *Cer1* mRNA in the embryos in (G) and (I) (H and J, respectively) immediately after in vitro culture.

Scale bars, 50 μm.

cues guide the transmigration of epiblast cells to the VE layer at the distal tip through local breaches in the BM barrier.

External Mechanical Cues Can Induce BM Breaches and Transmigration of Epiblast Cells Directly

To clarify the mechanism underlying the local thinning of the collagen IV deposition in the distal BM, we analyzed the expression profile of collagen IV genes. *Col4a1* mRNA and *Col4a2* mRNA were expressed throughout the primitive endoderm in the embryos at 4.5 dpc and then these mRNAs were restricted to the parietal endoderm, prominently around the boundary of the ExE and ectoplacental cone, with slight expression in the extraembryonic VE in the embryo at 5.5 dpc and cultured in the narrow and wide cavities (Figures S3C–S3F). These results suggest that the regionally restricted production of collagen IV in the proximal end and the enlargement of the surface area by the elongated egg cylinder shape may contribute to the distal thinning of the collagen IV deposition. To further assess how the BM is breached locally, we examined the possible involvement of matrix metalloproteinases (MMPs), which play a pivotal role for the disassembly of the extracellular matrix (Page-McCaw et al., 2007). The expressions of *Mmp2* and *Mmp9*, which primarily mediate the collagen IV degradation, and MMP activities monitored by MMP sense and DQ Collagen IV, fluorescent imaging agents, were only detected in the parietal endoderm of the embryos at stage 3 and cultured in the narrow and wide cavities (Figure S4). These results indicate that the local breach of the BM barrier at the distal tip is not dependent directly on proteolytic degradation by MMP activity.

To investigate whether external mechanical cues per se can breach the BM directly, we engineered deformed cavity devices that contained an extra cavity in the form of a bend at the end (Figure 7A) or an opening to the lateral side slightly above the end (Figure 7D) and cultured stage 1 embryos within these deformed cavities. After the 8 hr culture, the embryo proper did elongate along the cavity shape (Figures 7A and 7D), and the BM was breached toward the direction of the opened cavities ectopically, but not toward the distal side (Figures 7B and 7E). Furthermore, the VE cells in the vicinity of the BM breaches appeared to form nonsimple epithelial layers, suggesting the transmigration of epiblast cells (Figures 4N, 7C, and 7F). These results indicate that external spatial restriction exerted on the embryo can regulate the elongation of the egg cylinder and the location of BM breaches directly.

To evaluate the contribution of embryonic growth and external mechanical cues to the BM breach, stage 1 embryos were cultured in narrow cavities of 90 μm and even in much narrower cavities of 70 μm in diameter together with the administration of SB431542, an inhibitor of activin receptor-like kinase receptor-dependent signaling, i.e., TGF-β signaling (Figure 7G;

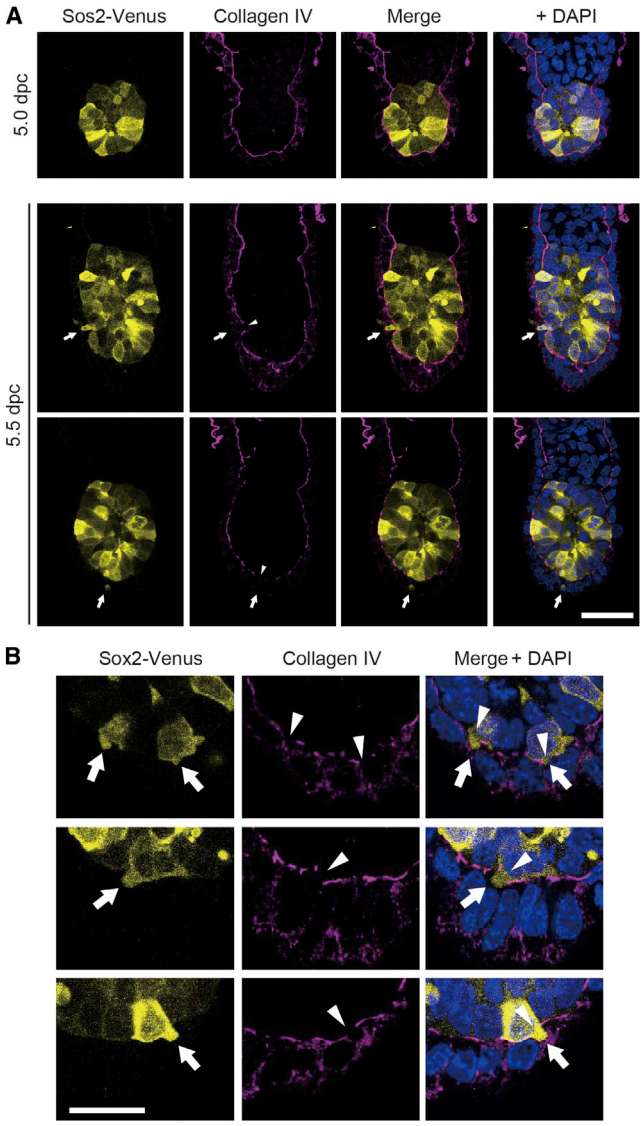

Figure 6. Behaviors of the Sox2-Venus-Positive Signal in the VE Layer

(A) Confocal images of Sox2-Venus (epiblast lineage, yellow) merged with anti-collagen IV (magenta) and DAPI (nuclei, blue) at 5.0 and 5.5 dpc. Arrows indicate the Sox2-Venus signal in the VE layer, and arrowheads indicate the location of the BM breach. Scale bar, 50 μm.

(B) Confocal images of Sox2-Venus (epiblast lineage, yellow) merged with anti-collagen IV (magenta) and DAPI (nuclei, blue) at the timing that the epiblast cells partially protrude into the VE layer beyond the BM. Arrows indicate the Sox2-Venus signal in the VE layer, and arrowheads indicate the location of the BM breach. Scale bar, 25 μm.

Yamamoto et al., 2009). The cell numbers for embryos in either the 90 or the 70 μm cavities were actually reduced by the SB431542 administration (209.33 ± 8.50 and 214.33 ± 10.41, respectively; n = 3; Figure S2A), which indicates that the treatment with SB431542 led to the impairment of proper cell proliferation in vitro. Under this condition, the ratio of the Co versus the Tr length for embryos cultured in the 90 μm cavity was 1.59, whereas that in the 70 μm cavity was 2.31, which is similar to that for the embryos at stage 3 in vivo and considered to constitute the elongated shape (Figure 7H). Concurrently, the collagen IV deposition was thinned in the distal region of embryos cultured in the 70 μm cavity, and the Sox2-Venus-positive cells were transmigrated to the VE layer (Figures 7J and 7J′). Conversely, in the embryos cultured in 90 μm cavities, collagen IV was heavily deposited throughout the BM, and no transmigrated cells were observed in the VE layer (Figure 7I). These results indicate that although sufficient embryonic growth is necessary for both the BM breach and the transmigration of epiblast cells, further increases in the external spatial restrictions can compensate for insufficient embryonic growth. In addition, although TGF-β signaling is shown to be required for correct DVE formation (Brennan et al., 2001; Yamamoto et al., 2004; Mesnard et al., 2006), the BM breach via mechanical cues did not appear to depend strictly upon TGF-β signaling. This finding suggests the primary and direct role of mechanical cues in the BM breach and transmigration of epiblast cells.

To further investigate whether mechanical cues affect the BM organization, we put local pressure on the distal tip of the embryo cultured in the wide cavity with an AFM cantilever and assessed the effect on the BM breach (Figure 7K). The exerted pressure was held at approximately 50 nN for 600 s (Figure 7L), and immediately after the pressing, the BM of embryos was analyzed. In the embryo without pressing, collagen IV was heavily deposited throughout the BM, which was consistent with the above findings (n = 6; Figures 7M and 4D). Conversely, in the embryo with pressing, the distal surface of the embryo was dented at the pressure site (Figures 7N and 7N′, arrowheads), the BM was breached, and moreover, the epiblast cells toward the VE layer were protruded at both sides of the pressing location in some embryos (n = 2/8, both breach and protrusion; n = 2/8, solely distortion of the BM; Figures 7N and 7N′, arrows). These results indicate that external mechanical stress can affect the local BM breach directly. Taken together with the aforementioned findings, these results suggest that mechanical cues arising from the appropriate physical growth of embryos in size and external geometrical constraints regulate the local breach of the BM and transmigration of epiblast cells into the VE layer directly.

DISCUSSION

Previous studies have revealed crucial molecular pathways and cellular behaviors for A-P axis polarization in mouse development (Arnold and Robertson, 2009; Rossant and Tam, 2009; Takaoka and Hamada, 2012). However, these studies have focused on events within the embryo itself, and there is still little knowledge about the role of external cues provided by maternal tissue and dynamic interactions between tissue layers during the early implantation stage. In the present study, we demonstrated, through the use of microcavity-engineered embryo cultures, that external mechanical cues exerted on embryos are crucial for postimplantation development, i.e., A-P axis polarization. In addition, elongation of the egg cylinder shape and DVE formation are not simply embryo autonomous but rather require external forces guiding directional embryonic growth. The mechanical cues induce local breach of the BM barrier at the distal tip and consequently induce DVE formation through transmigration of

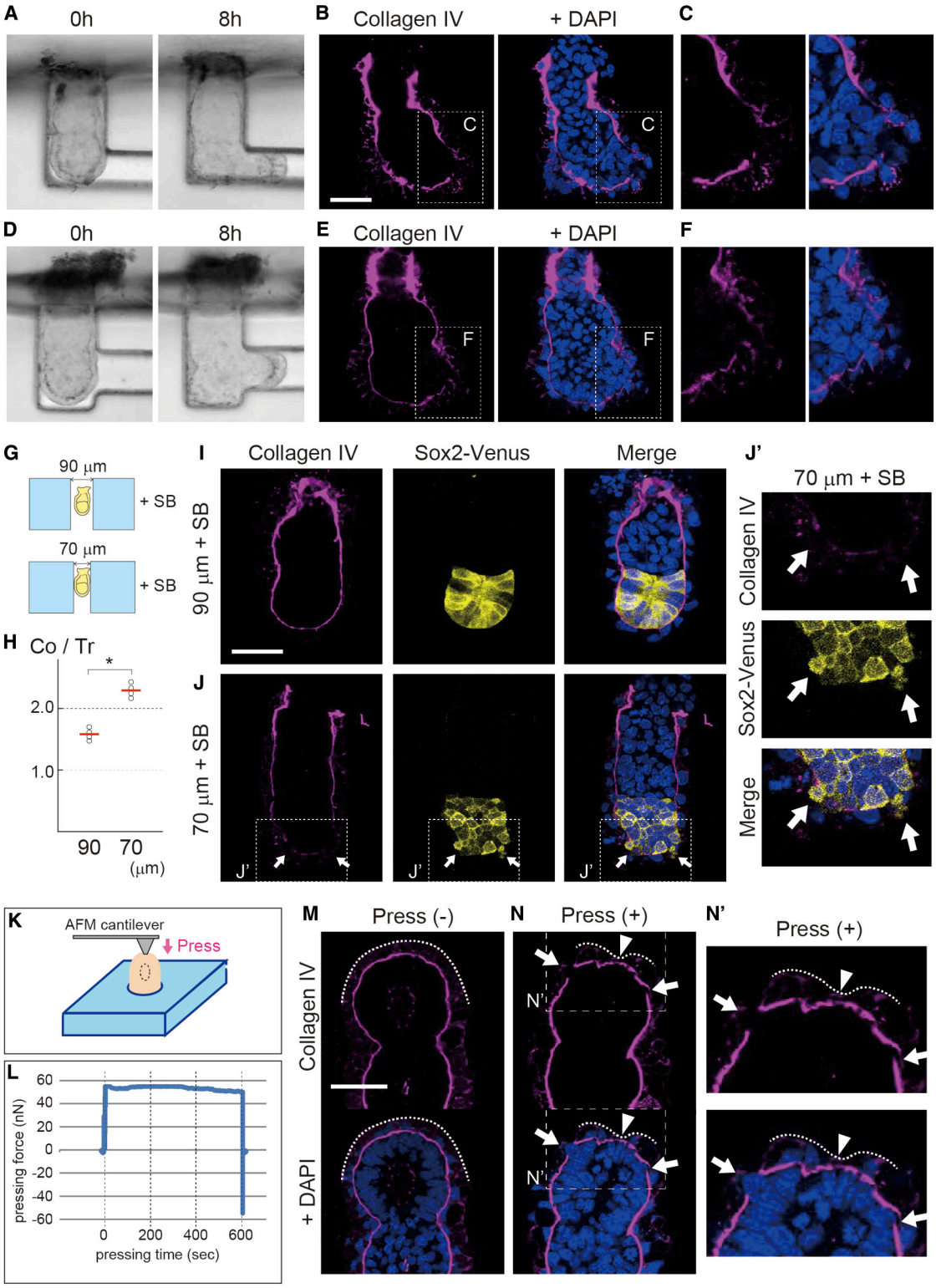

Figure 7. External Mechanical Cues Regulate Localized BM Breach and Transmigration of Epiblast Cells

(A and D) Embryos inserted in ectopic cavity devices before culture (0 hr) and after 8 hr culture (8 hr).

(B, C, E, and F) Immunohistochemical analysis of anti-collagen IV (magenta) merged with DAPI (nuclei, blue) in the embryo cultured for 8 hr. (C) and (F) show higher magnifications of the areas in (B) and (E), respectively.

(G) A schematic representation showing the embryo culture in 90 and 70 μm cavities with the administration of SB431542.

(legend continued on next page)

the epiblast cells into the VE layer. Additionally, these findings also provide unique insights into why the first axis polarity of the mouse embryo is established in the P-D direction, but not in the future A-P direction.

Mechanical Mechanism by which the Elongated Shape of the Egg Cylinder Induces BM Breaches and Transmigration of Epiblast Cells Locally at the Distal Tip

How does an external mechanical force induce DVE formation in the distal portion of the egg cylinder? Our findings suggest that external mechanical force by an embryo-extrinsic environment can direct the selective growth of embryos along the P-D direction and consequently give rise to an elongated shape from a bowl-like shape of the egg cylinder (Figure 8A). This selective growth may increase the biomechanical stress acting on the distal region away from the proximal region, where BM proteins are produced, to the distal region. Therefore, the BM at the distal portion will tend to breach, and the cell migration from epiblast to VE will be promoted (Figures 6B and 8A).

Additionally, the bending moment is also consistent with the localized BM breaches at the distal portion (Figure 8B). Given that the epiblast and the BM are simply a curved plate structure, the maximum bending stress exists at the center of the plate, i.e., at the distal tip of the embryo. Furthermore, the bending stress is theoretically increased inversely with the radius of curvature of the embryo, i.e., it is estimated that the stress acting on the embryo cultured in the narrow cavity is stronger than that of the embryo cultured in the wide cavity. Therefore, it can be considered that the bending stress reacts maximally at the distal tip in the embryo cultured in the narrow cavity (Figure 8B; Young and Budynas, 2002). These mechanical explanations can provide a rational understanding of why the external mechanical force rather than specific molecular pathways can induce the localized BM breaches at the distal portion and consequent transmigration of epiblast cells. Moreover, this mechanical model may provide a good explanation for the stochastic nature of *Cer1* expression, which exhibits a slight lateral tilt but not at the exact center of the distal tip during DVE formation.

One of the unexpected findings reported here is that a small number of cells transmigrated from the epiblast contribute to the DVE at 5.5 dpc (Figures 5 and 6). This finding is in good agreement with previous morphological observations (Thomas et al., 1998; Kimura et al., 2000). The VE cells at the distal tip had a more columnar morphology and contained a large oval nucleus as well as prominent nucleoli, which appear to be different from other typical VE cells that consist of a simple cuboidal epithelium having large vacuoles and a small flat nucleus (Kimura et al., 2000). The current study provides direct evidence for the distinct developmental origins of DVE cells. However, there was only a small number of epiblast-derived β-gal-positive cells among the Cer1-positive cells that were predicted to join the AVE at 6.5 dpc (approximately four cells), and this number could hardly account for all the AVE cells. Indeed, *Cer1* expression was evident in AVE cells outside of the epiblast-derived β-gal-positive cells (Figure 5). This finding also suggests that AVE formation is attributable to not only the epiblast-transmigrated cells directly but also non-cell-autonomous mechanisms through diffusible or cell surface factors after BM breaches. Additionally, because the subset of VE cells is capable of contributing to definitive endoderm cells during gastrulation (Kwon et al., 2008), it might be worth investigating in the future whether the apparent fate heterogeneity within the VE cells is attributable to epiblast-derived DVE cells identified in the present study.

External Mechanical Cues Establish A-P Axis Polarization

Considering the aforementioned findings together, we propose a fascinating hypothesis for DVE formation via external mechanical cues (Figure 8A). After implantation, the uterine endometrium quickly undergoes a decidual reaction upon attachment of the embryo. In addition to the invasion and spread of the embryonic components into the uterine mucosa, the uterine epithelium folds up to enclose the embryo. The uterine epithelium structure is not fused completely at stage 1 (5.0 dpc) but participates in forming an oblong cavity for the embryo (Figures 1C and 1E). Therefore, the yolk sac cavity surrounding the embryo is not firmly formed yet, and the embryo can grow out in all directions (5.0 dpc; Figure 8A, shown by a dashed square). Because the uterine epithelium is degenerated, and the decidual cells surround the embryo closely at stage 3 (5.5 dpc), however, there is little space between the embryo and the wall of the yolk sac cavity except at the distal side of the embryo (Figures 1C and 1E). Additionally, a sufficient stiffness of the maternal tissues surrounding the embryo, around 20 kPa (Figure 3), is formed due to the proper decidual reaction. Accordingly, the reaction force of maternal tissue may restrict the growth of the embryo mechanically in the Tr direction at stage 3 (5.5 dpc; Figure 8A, shown in dashed rectangles).

In the current study, impairment of cell proliferation was shown to lead to a failure in DVE formation, which may be primarily brought about by reducing mechanical forces to expand the embryo in the distal direction (Figures 7G–7J′). In good agreement with this notion, genetic mutations in Nodal and Smad signalings have been shown to lead to the ectopic deposition of the BM between the epiblast and VE layer (Figures 7G–7J′; Costello et al., 2009; Mesnard et al., 2006) and impairment of epiblast growth as well as DVE formation (Brennan et al., 2001; Yamamoto et al., 2004; Stuckey et al., 2011; Mesnard et al., 2006;

(H) The ratio of the Co versus the Tr lengths in 90 and 70 μm cavities with SB. Red lines indicate the mean value of each ratio. *$p < 0.01$.
(I–J′) Immunohistochemical analysis of anti-collagen IV (magenta) merged with DAPI (nuclei, blue) in *Sox2-Venus* (yellow) transgenic embryos cultured for 8 hr. (J′) shows higher magnifications of the areas in (J). Arrows indicate the BM breach and protrusion of epiblast cells (J and J′).
(K) A schematic representation showing local pressing at the distal region of the embryo cultured in the wide cavity with an AFM probe.
(L) The force graph of pressing by the AFM probe. Subzero forces immediately after finishing the pressing (600 s) indicate that the pressed site of the embryo was pulled up together with the pull-up of the AFM probe to some degree.
(M–N′) Immunohistochemical analysis of anti-collagen IV (magenta) merged with DAPI (nuclei, blue) in the embryo cultured for 8 hr. (N′) shows higher magnifications of the areas in (N). Arrowheads indicate the pressed site by AFM. Arrows indicate the breach of BM and protrusion of epiblast cells.
The cavity used in (A)–(C) is L-shaped with a bend at the end, and the cavity used in (D)–(F) has openings slightly above the end. Scale bars, 50 μm. See also Figures S2 and S4.

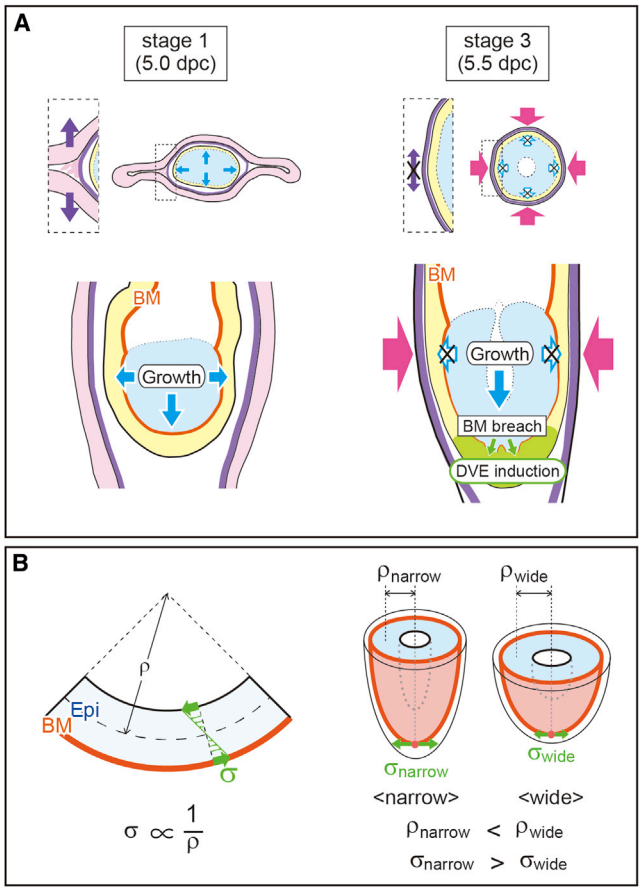

Figure 8. Schematic Model of the Mechanism of DVE Formation by Mechanical Stress

(A) At stage 1 (5.0 dpc), the embryonic growth is not restricted by the external maternal tissue. At stage 3 (5.5 dpc), the embryonic growth is restricted mechanically. Therefore, the embryo elongates along the P-D direction, and the BM at the distal part of the embryo is breached to induce transmigration of epiblast cells into the VE layer, thereby forming the DVE. Light blue indicates the epiblast, yellow indicates the VE layer, green indicates the DVE, red lines indicate the BM, light magenta indicates the uterine epithelium, dark magenta indicates the parietal endoderm layer, blue arrows point in the direction of the embryo expansion, magenta arrows point to the reaction force of the decidual tissue against the embryo, and dark magenta arrows point to the expansion of the yolk sac cavity at the hinge region. The upper and lower illustrations are Tr and sagittal images of the embryo and the yolk sac cavity, respectively.

(B) Schematic presentations of the bending moment acting in the embryo cultured with or without external force. Red lines and light-red areas indicate the BM, light-blue areas indicate the epiblast layer (Epi), and σ and green arrows point to bending stress. ρ, radius of curvature.

Clements et al., 2011). These several lines of genetic evidence are coherent with our model, in which mechanical forces due to the proper embryonic growth are crucial for the BM breach and subsequent DVE formation.

Surgical ablation of the ExE or the genetic mouse mutations regulating development of the ExE, such as *Bmp4* and *Apc* mutations, are known to lead to aberrant upregulation or loss of DVE marker expression (Rodriguez et al., 2005; Richardson et al., 2006; Chazaud and Rossant, 2006; Soares et al., 2008). In the current model, given that ectopic deposition and thinning of the BM intimately affect DVE formation (Figures 4 and S3), it may be considered that loss of the ExE architecture may drastically affect the deposition and thinning of the BM and that the expression of DVE markers may be thereby altered. Alternatively, the growth of the ExE itself may act as an important mechanical factor for the elongated shape of the egg cylinder, i.e., by turning the growth of the epiblast toward the distal direction, but not toward the proximal direction. Consistent with this hypothesis, the trophoblast growth in the proximal portion has been shown to be required for correct egg cylinder morphogenesis in vitro (Copp, 1981). These several lines of evidence suggest the possibility that the structural element of ExE may be necessary for the spatial limitation in the proximal direction as well as the correct deposition and breach of the BM.

Due to the unique character of mammalian development, the effect of the uterine environment on embryogenesis has been considered. Our current study shows that in addition to the maternal nutrition supply, the maternal tissue itself is essential for normal embryonic morphogenesis in mammals. McLaren and Michie described that the number of lumber vertebrae of mice developing from reciprocally transferred embryos resembled their foster mothers rather than their genetic mothers by using the technique of embryo transfer, which suggests that the uterine environment influences the anatomical characteristics of the embryo (McLaren and Michie, 1958). To our knowledge, the present study is the first to show that the mechanical environment outside of the embryo directly triggers formation of the initial body axis, i.e., A-P axis polarization, which is one of the fundamental processes during development. Further investigations into the mechanisms encompassing the mechanical environment outside of the embryo will significantly advance our understanding of mammalian embryogenesis.

EXPERIMENTAL PROCEDURES

Fabrication of the Microcavity Device

The microcavity device was fabricated by curing PDMS prepolymer (Dow Sylgard 184; 10:1 polymer to curing agent) against a photolithographically prepared SU-8 (Epoxy-based photoresist; MicroChem) mold containing a positive pattern of cylinder (diameter, 90 μm for the narrow cylinder and 180 μm for the wide cylinder; height, over 500 μm) at 60°C overnight. The cured PDMS was carefully peeled off the mold and used as the microcavity device in this experiment.

Measurement of the Modulus of Agarose Gel

Stiffness of agarose gel was measured by using a Texture Analyzer (TA.XTplus; Stable Micro Systems). The measuring condition was performed with a 0.5-in-diameter cylindrical probe. Briefly, agarose was purchased from Bioline (catalog, Bio-41026). Four variations of agarose in culture medium (see below) were prepared at concentrations of 0.3%, 0.5%, 0.8%, and 1% w/v in 35 mm dishes. These agarose gels were compressed at a 0.2 mm/s deformation rate. The resulting force-displacement curves were used to characterize mechanical properties of the gels, using a Hertzian contact model for indentation measurements.

AFM

Decidual tissues excised from the uterus at 5.5 dpc were teased apart, and the embryo was removed with fine forceps taking care not to scratch the surface of the side attached to the embryo. Tissues attached to the embryo were cut, and the thickness of the tissue was confirmed by light microscopy to be thinner than 200 μm. Dissected tissues were kept in medium, DMEM/F-12 (Life Technologies) supplemented with 10% fetal cow serum (Thermo Scientific), 0.01M HEPES, and penicillin/streptomycin (Life Technologies). The tissue

was transferred on a 35 mm dish with the medium, glued to the dish putting the surface attached with the embryo up, and probed by the AFM tip. A Nanowizard III BioAFM (JPK Instruments) was used for the force spectroscopy. The head unit and stage of the AFM were set on an inverted microscope (IX70; Olympus), and laser alignment was achieved with a CCD camera. A commercially available silicon AFM tip (ATEC-CONT, Nanosensors; spring constant, 0.2 N/m) was used for the decidual tissue force spectroscopy at room temperature. For force spectroscopy, the spring constant of every cantilever was calibrated using the energy equipartition theorem. The loading speed for force spectroscopy was 8 μm/s at the 4 μm piezo travel length. All force-distance curves were processed in order to determine the tissue Young's modulus measurements with a batch-processing program that was included in the AFM software. For the external indentation of ECM using AFM, the real-time force spectroscopy was achieved after the AFM tip spring constant calibration. The indentation force was monitored and controlled manually using the stepping motor of head unit.

Whole-Embryo Culture in the Microcavity

The wild-type, *Cer1-EGFP*, and *Sox2-Venus* embryos at stage 1 (approximately 5.0 dpc embryos, in which a proamniotic cavity was not clearly observed) were collected in the warmed DMEM/F-12 supplemented with 10% fetal cow serum, 0.01 M HEPES, and penicillin/streptomycin. The parietal endoderm of embryos was cut at the distal side and remained attached on the prospective ectoplacental cone. Stage 1 embryos were inserted into the microcavity of the PDMS device or agarose gel and cultured in DMEM/F-12 medium containing 50% rat serum and penicillin/streptomycin in a 5% CO_2 incubator at 37°C for 8–24 hr. Some embryos were cultured in medium containing collagenase D (500 μg/ml; Roche) or SB431542 (20 μmol/l; Sigma-Aldrich) for 8 hr. Cultured embryos were subjected to histological, immunohistochemical, and RNA analyses as described in the Supplemental Experimental Procedures.

Ethics Statement

All mouse studies followed the fundamental guidelines for proper conduct of animal experiment and related activities in academic research institutions under the jurisdiction of the Ministry of Education, Culture, Sports, Science and Technology in Japan and are approved by the institutional Committees at the Osaka Medical Center and Research Institute for Maternal and Child Heath for animal experiments.

ACCESSION NUMBERS

The accession number for the microarray data reported in this paper is GSE51198.

SUPPLEMENTAL INFORMATION

Supplemental Information includes Supplemental Experimental Procedures, four figures, and one table and can be found with this article online at http://dx.doi.org/10.1016/j.devcel.2013.09.026.

ACKNOWLEDGMENTS

We are grateful to C. Moraes, K. Shimokawa, and S. Amazaki for their technical support and E. DeRobertis, B. Hogan, H. Sasaki, H. Hamada, J. Deschamps, K. Yamamura, M.M. Shen, R. Beddington, H. Schoeler, J. Belo, A. Miyawaki, T. Nagai, and H. Niwa for the plasmids. This work was supported in part by a Grant-in-Aid for Scientific Research on Innovative Areas from the Ministry of Education, Culture, Sports, Science and Technology, Japan, and by grants from the Naito Foundation, the Uehara Memorial Foundation, and the Takeda Science Foundation. R.H. is a research fellow of the Japan Society for the Promotion of Science (SPD).

Received: February 6, 2013
Revised: July 16, 2013
Accepted: September 27, 2013
Published: October 28, 2013

REFERENCES

Arnold, S.J., and Robertson, E.J. (2009). Making a commitment: cell lineage allocation and axis patterning in the early mouse embryo. Nat. Rev. Mol. Cell Biol. *10*, 91–103.

Beddington, R.S., and Robertson, E.J. (1999). Axis development and early asymmetry in mammals. Cell *96*, 195–209.

Brennan, J., Lu, C.C., Norris, D.P., Rodriguez, T.A., Beddington, R.S., and Robertson, E.J. (2001). Nodal signalling in the epiblast patterns the early mouse embryo. Nature *411*, 965–969.

Chazaud, C., and Rossant, J. (2006). Disruption of early proximodistal patterning and AVE formation in Apc mutants. Development *133*, 3379–3387.

Clements, M., Pernaute, B., Vella, F., and Rodriguez, T.A. (2011). Crosstalk between Nodal/activin and MAPK p38 signaling is essential for anterior-posterior axis specification. Curr. Biol. *21*, 1289–1295.

Copp, A.J. (1981). The mechanism of mouse egg-cylinder morphogenesis in vitro. J. Embryol. Exp. Morphol. *61*, 277–287.

Costello, I., Biondi, C.A., Taylor, J.M., Bikoff, E.K., and Robertson, E.J. (2009). Smad4-dependent pathways control basement membrane deposition and endodermal cell migration at early stages of mouse development. BMC Dev. Biol. *9*, 54.

Engler, A.J., Griffin, M.A., Sen, S., Bönnemann, C.G., Sweeney, H.L., and Discher, D.E. (2004). Myotubes differentiate optimally on substrates with tissue-like stiffness: pathological implications for soft or stiff microenvironments. J. Cell Biol. *166*, 877–887.

Hayashi, S., Lewis, P., Pevny, L., and McMahon, A.P. (2002). Efficient gene modulation in mouse epiblast using a Sox2Cre transgenic mouse strain. Gene Expr. Patterns *2*, 93–97.

Janmey, P.A., and Miller, R.T. (2011). Mechanisms of mechanical signaling in development and disease. J. Cell Sci. *124*, 9–18.

Kemp, C.R., Willems, E., Wawrzak, D., Hendrickx, M., Agbor Agbor, T., and Leyns, L. (2007). Expression of Frizzled5, Frizzled7, and Frizzled10 during early mouse development and interactions with canonical Wnt signaling. Dev. Dyn. *236*, 2011–2019.

Kimura, C., Yoshinaga, K., Tian, E., Suzuki, M., Aizawa, S., and Matsuo, I. (2000). Visceral endoderm mediates forebrain development by suppressing posteriorizing signals. Dev. Biol. *225*, 304–321.

Kimura-Yoshida, C., Nakano, H., Okamura, D., Nakao, K., Yonemura, S., Belo, J.A., Aizawa, S., Matsui, Y., and Matsuo, I. (2005). Canonical Wnt signaling and its antagonist regulate anterior-posterior axis polarization by guiding cell migration in mouse visceral endoderm. Dev. Cell *9*, 639–650.

Kwon, G.S., Viotti, M., and Hadjantonakis, A.K. (2008). The endoderm of the mouse embryo arises by dynamic widespread intercalation of embryonic and extraembryonic lineages. Dev. Cell *15*, 509–520.

Lu, C.C., Robertson, E.J., and Brennan, J. (2004). The mouse frizzled 8 receptor is expressed in anterior organizer tissues. Gene Expr. Patterns *4*, 569–572.

Mammoto, T., and Ingber, D.E. (2010). Mechanical control of tissue and organ development. Development *137*, 1407–1420.

McLaren, A., and Michie, D. (1958). Factors affecting vertebral variation in mice. 4. Experimental proof of the uterine basis of a maternal effect. J. Embryol. Exp. Morphol. *6*, 645–659.

Mesnard, D., Filipe, M., Belo, J.A., and Zernicka-Goetz, M. (2004). The anterior-posterior axis emerges respecting the morphology of the mouse embryo that changes and aligns with the uterus before gastrulation. Curr. Biol. *14*, 184–196.

Mesnard, D., Guzman-Ayala, M., and Constam, D.B. (2006). Nodal specifies embryonic visceral endoderm and sustains pluripotent cells in the epiblast before overt axial patterning. Development *133*, 2497–2505.

Page-McCaw, A., Ewald, A.J., and Werb, Z. (2007). Matrix metalloproteinases and the regulation of tissue remodelling. Nat. Rev. Mol. Cell Biol. *8*, 221–233.

Perea-Gomez, A., Vella, F.D., Shawlot, W., Oulad-Abdelghani, M., Chazaud, C., Meno, C., Pfister, V., Chen, L., Robertson, E., Hamada, H., et al. (2002). Nodal antagonists in the anterior visceral endoderm prevent the formation of multiple primitive streaks. Dev. Cell *3*, 745–756.

Potts, D.M. (1968). The ultrastructure of implantation in the mouse. J. Anat. *103*, 77–90.

Richardson, L., Torres-Padilla, M.E., and Zernicka-Goetz, M. (2006). Regionalised signalling within the extraembryonic ectoderm regulates anterior visceral endoderm positioning in the mouse embryo. Mech. Dev. *123*, 288–296.

Rodriguez, T.A., Srinivas, S., Clements, M.P., Smith, J.C., and Beddington, R.S. (2005). Induction and migration of the anterior visceral endoderm is regulated by the extra-embryonic ectoderm. Development *132*, 2513–2520.

Rossant, J., and Tam, P.P. (2004). Emerging asymmetry and embryonic patterning in early mouse development. Dev. Cell *7*, 155–164.

Rossant, J., and Tam, P.P. (2009). Blastocyst lineage formation, early embryonic asymmetries and axis patterning in the mouse. Development *136*, 701–713.

Shawlot, W., Min Deng, J., Wakamiya, M., and Behringer, R.R. (2000). The cerberus-related gene, Cerr1, is not essential for mouse head formation. Genesis *26*, 253–258.

Shimokawa, K., Kimura-Yoshida, C., Nagai, N., Mukai, K., Matsubara, K., Watanabe, H., Matsuda, Y., Mochida, K., and Matsuo, I. (2011). Cell surface heparan sulfate chains regulate local reception of FGF signaling in the mouse embryo. Dev. Cell *21*, 257–272.

Smith, L.J. (1985). Embryonic axis orientation in the mouse and its correlation with blastocyst relationships to the uterus. II. Relationships from 4 1/4 to 9 1/2 days. J. Embryol. Exp. Morphol. *89*, 15–35.

Soares, M.L., Torres-Padilla, M.E., and Zernicka-Goetz, M. (2008). Bone morphogenetic protein 4 signaling regulates development of the anterior visceral endoderm in the mouse embryo. Dev. Growth Differ. *50*, 615–621.

Soriano, P. (1999). Generalized lacZ expression with the ROSA26 Cre reporter strain. Nat. Genet. *21*, 70–71.

Srinivas, S., Rodriguez, T., Clements, M., Smith, J.C., and Beddington, R.S. (2004). Active cell migration drives the unilateral movements of the anterior visceral endoderm. Development *131*, 1157–1164.

Stuckey, D.W., Di Gregorio, A., Clements, M., and Rodriguez, T.A. (2011). Correct patterning of the primitive streak requires the anterior visceral endoderm. PLoS One *6*, e17620.

Takaoka, K., and Hamada, H. (2012). Cell fate decisions and axis determination in the early mouse embryo. Development *139*, 3–14.

Takaoka, K., Yamamoto, M., Shiratori, H., Meno, C., Rossant, J., Saijoh, Y., and Hamada, H. (2006). The mouse embryo autonomously acquires anterior-posterior polarity at implantation. Dev. Cell *10*, 451–459.

Thomas, P., and Beddington, R. (1996). Anterior primitive endoderm may be responsible for patterning the anterior neural plate in the mouse embryo. Curr. Biol. *6*, 1487–1496.

Thomas, P.Q., Brown, A., and Beddington, R.S. (1998). Hex: a homeobox gene revealing peri-implantation asymmetry in the mouse embryo and an early transient marker of endothelial cell precursors. Development *125*, 85–94.

Torres-Padilla, M.E., Richardson, L., Kolasinska, P., Meilhac, S.M., Luetke-Eversloh, M.V., and Zernicka-Goetz, M. (2007). The anterior visceral endoderm of the mouse embryo is established from both preimplantation precursor cells and by de novo gene expression after implantation. Dev. Biol. *309*, 97–112.

Yamamoto, M., Saijoh, Y., Perea-Gomez, A., Shawlot, W., Behringer, R.R., Ang, S.L., Hamada, H., and Meno, C. (2004). Nodal antagonists regulate formation of the anteroposterior axis of the mouse embryo. Nature *428*, 387–392.

Yamamoto, M., Beppu, H., Takaoka, K., Meno, C., Li, E., Miyazono, K., and Hamada, H. (2009). Antagonism between Smad1 and Smad2 signaling determines the site of distal visceral endoderm formation in the mouse embryo. J. Cell Biol. *184*, 323–334.

Young, W.C., and Budynas, R.D. (2002). Roark's Formulas for Stress and Strain (New York: McGraw-Hill).